

## Negative Heat Capacity for a Cluster of 147 Sodium Atoms

Martin Schmidt, Robert Kusche, Thomas Hippler, Jörn Donges, Werner Kronmüller,  
Bernd von Issendorff, and Hellmut Haberland

*Fakultät für Physik, Universität Freiburg, H.Herderstrasse 3, D-79104 Freiburg, Germany*

(Received 24 July 2000)

There exists a surprising theoretical prediction for a small system: its microcanonical heat capacity can become negative. An increase of energy can—under certain conditions—lead to a lower temperature. Here we present experimental evidence that a cluster containing exactly 147 sodium atoms does indeed have a negative microcanonical heat capacity near its solid to liquid transition.

DOI: 10.1103/PhysRevLett.86.1191

PACS numbers: 36.40.Ei

Every day experience tells us that if one adds energy to a system it will get warmer. But negative heat capacities have long since been known in astrophysics [1,2], where energy can be added to a star or star cluster which then cools down. A similar effect has been calculated for melting atomic clusters [3,4] and fragmenting nuclei [5]; in the latter case it has been observed as well [6].

We have recently developed a method to study thermal properties of free, mass selected clusters [7–11]. Briefly, photofragmentation is used to measure the internal energy of clusters with known temperature. The experimental procedure can be divided into two steps: (1) Cluster ions are produced in a gas aggregation source and thermalized in helium gas of controlled temperature  $T$ , which represents an ideal heat bath. A mass spectrometer is used to select a single cluster size. This prepares clusters of known size and known temperature  $T$ . (2) These clusters are irradiated by a laser beam. They absorb photons of well defined energy, which leads to stepwise increase of the internal energy of the cluster and eventually to evaporation of several atoms. A second mass spectrometer measures the distribution of the fragments produced, which has a characteristic shape as shown in Fig. 1. Different numbers of absorbed photons lead to clearly separated groups of fragments in the mass distribution. The number of evaporated atoms depends on the total inner energy of the cluster, which is the sum of the original thermal energy plus the energy of the absorbed photons. If the temperature of the heat bath is varied, the inner energy of the selected cluster changes and thus also the number of evaporated atoms. The fragment groups shift on the mass scale as shown in Fig. 2. This allows one to determine the caloric curve and its derivative, the heat capacity. This form of data evaluation is an improvement of the one used earlier [7–9,12] and is described in [13].

For the determination of the caloric curves we have used so far only the positions of the fragment groups. As will become obvious from the discussion below, a negative heat capacity cannot be observed in this case. One thus needs more information, which can be obtained from the measured fragment distributions. In fact, the fragment group envelopes are maps of the energy distribution, as indicated

in Fig. 1. As the clusters have been thermalized in a heat bath, they have a canonical distribution of inner energies  $P_T(E)$  which is proportional to the number of accessible states  $\Omega(E)$  times the Boltzmann factor [14]:

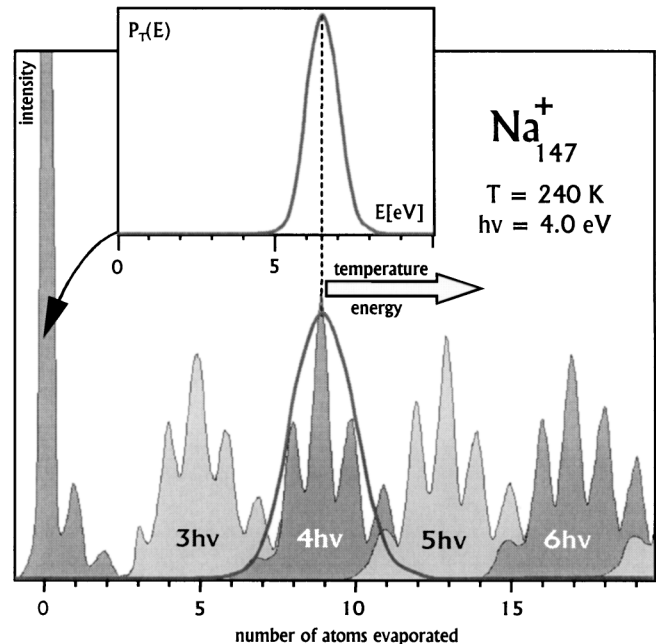


FIG. 1. The energy distribution of a free cluster can be obtained from its photofragmentation mass spectrum. In the experiment a  $\text{Na}_{147}^+$  cluster ejects atoms after absorption of several photons. The intensity of the charged fragments is plotted against the number of evaporated atoms. Without laser interaction one observes only the large peak on the left, corresponding to the intact  $\text{Na}_{147}^+$ . For four absorbed photons one has an approximately Gaussian distribution centered around nine evaporated atoms. For five (six) absorbed photons the Gaussian would be centered near 13 (17) ejected atoms. The distance between the maxima of the Gaussians corresponds to exactly one photon energy, which provides an energy calibration of the mass scale. The more energy a cluster carries before photoexcitation the more atoms it will evaporate afterwards. Thus, the mass distribution (thick solid line) corresponding to a fixed number of absorbed photons is a map of its internal energy distribution  $P_T(E)$ , as shown in the inset. As the cluster has been thermalized in a heat bath,  $P_T(E)$  is a canonical energy distribution as given by Eq. (1).

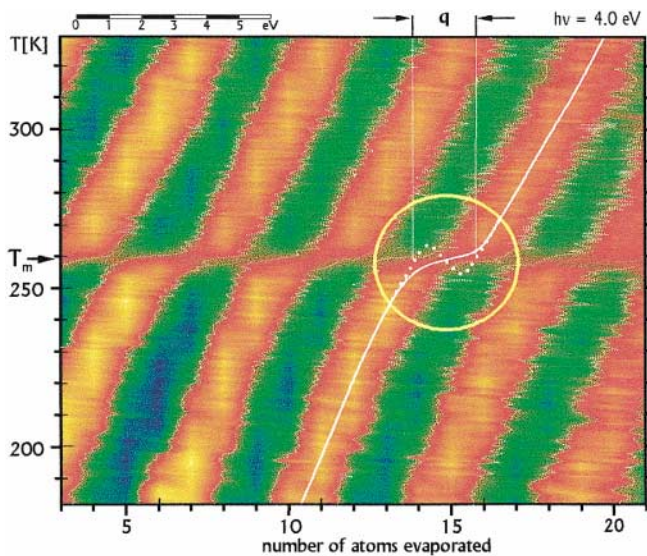


FIG. 2 (color). Plotting the envelope of the fragment mass intensities of Fig. 1 as a function of the cluster's temperature gives a two-dimensional presentation of the primary data (red, high intensity). The progression of the intensity maxima represents a smoothed microcanonical caloric curve (white solid line, see text and Fig. 3 for details). Heat capacity, melting temperature, and latent heat  $q$  can be deduced. Because of an experimental broadening effect the backbending (dotted line) is smoothed out.

$$P_T(E) \propto \Omega(E) \exp(-E/k_B T) = \exp(S/k_B - E/k_B T), \quad (1)$$

where  $S = k_B \ln(\Omega)$  is the entropy of the system.

The function  $P_T(E)$  carries the full thermodynamical information. Both canonical and microcanonical thermodynamics can be derived from it. The canonical caloric curve is a plot of the mean energy  $\langle E \rangle = \int E P_T(E) dE$  against the heat bath temperature  $T$ . This curve is strictly monotonously increasing. Its heat capacity is thus always positive as can be proven analytically [1,2,14,15].

The microcanonical caloric curve is defined differently. It is the curve one would obtain if one measures the temperature of an isolated cluster (using an infinitesimally small thermometer) as a function of its energy. As clusters with a range of energies leave the source, they have also a range of microcanonical temperatures  $T_\mu$ . Differentiating Eq. (1) with respect to the energy, one sees that the condition for an extremum of  $P_T(E)$  is identical to the definition [14] of  $T_\mu$ :

$$T = (\partial S / \partial E)^{-1} \equiv T_\mu. \quad (2)$$

Thus, if the canonical energy distribution  $P_T(E)$  has an extremum at energy  $E_{\text{ext}}$  then the corresponding  $T_\mu$  equals  $T$ . In other words, a cluster with energy  $E_{\text{ext}}$  has a microcanonical temperature equal to  $T$ . One can thus obtain the microcanonical caloric curve by plotting  $E_{\text{ext}}$  against the heat bath temperature  $T$ , which can be done from the data given in Fig. 2.

Normally the difference between the canonical and the microcanonical caloric curve is minute. Far from a phase

transition the distribution  $P_T(E)$  is nearly Gaussian (see inset of Fig. 1) and thus the mean energy  $\langle E(T) \rangle$  and the most probable energy  $E_{\text{ext}}(T)$  are almost identical.

This is not true any more near a phase transition. The entropy  $S(E)$  of a small system can exhibit a curious structure here, a dent with an inverted curvature as shown in Fig. 3. This structure has been predicted by theory and has been observed in many numerical simulations [3–5,16,17]. The inverted curvature of the entropy has two interesting consequences (cf. Fig. 3): (1) The microcanonical caloric curve  $T_\mu(E)$  gets a negative slope (colloquially called backbending), which means that the corresponding heat capacity becomes negative. (2) The canonical energy distribution  $P_T(E)$  shows a bimodal structure [17,18].

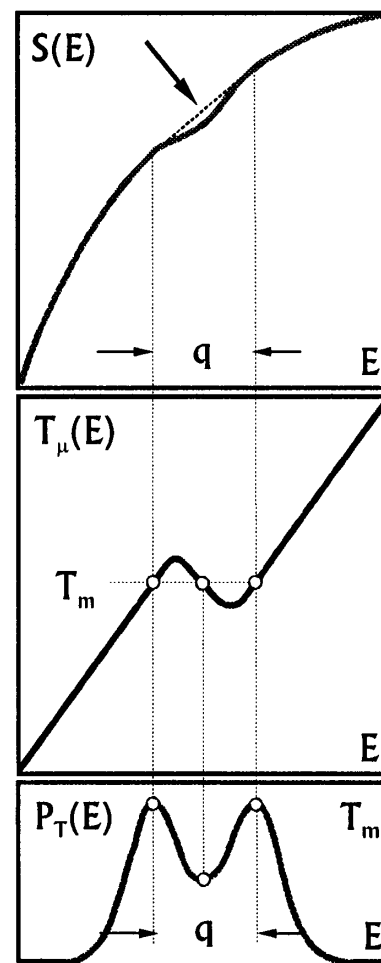


FIG. 3. Three quantities are plotted as a function of the inner energy of a cluster, illustrating different manifestations of the same phenomenon ( $q$  is the latent heat,  $T_m$  the melting temperature). Top: The total entropy  $S(E)$  having an inverted curvature dent (arrow), which is strongly exaggerated here. Such a structure is theoretically expected for a small particle. Middle: A backbending microcanonical caloric curve. The heat capacity becomes negative in the region with the negative slope. Bottom: The energy distribution  $P_T(E)$  [see Eq. (1)] of a cluster ensemble close to its melting temperature. Because of the inverted curvature of the entropy the distribution becomes bimodal.

Since  $P_T(E)$  is mapped onto the shape of the fragment groups, these should become bimodal, too. An observation of the bimodality would therefore be a direct proof of a negative heat capacity. Fragment distributions were studied in detail for  $\text{Na}_{147}^+$ , a cluster for which the effect of a negative heat capacity can be expected to be particularly pronounced due to its very high latent heat [8,9,17]. Unfortunately, the bimodality could not be observed directly, as there are broadening mechanisms in the fragmentation process which just smear out these details [19]. We thus had to apply a trick which enhances the modulation of the fragment spectra: for a certain photon energy the overlap of adjoining fragment groups produces a pattern which allows one an unambiguous decision whether or not the microcanonical caloric curve shows backbending.

This will be discussed with the help of Fig. 4. Its top line shows three examples of model (microcanonical) caloric curves. They are identical except at the transition itself. The middle column of Fig. 4 shows the steplike progression of macroscopic systems. On the left side a smoothed out caloric curve is shown, and in the right column the backbending progression as suggested by Fig. 3 and the arguments given above. Using Eqs. (1) and (2), one can calculate the corresponding energy distributions  $P_T(E)$  at the melting temperature  $T_m$ , which are shown in the second row of Fig. 4. In the case of the steplike caloric curve the distribution is Gaussian on the rising and falling edges and completely flat at the top. The width of the hatched rectangle which has the same area as  $P_T(E)$  is given by

$$\Gamma = T\sqrt{2\pi k_B c} + q. \quad (3)$$

The first term is due to the canonical energy distribution [14] at temperature  $T$ , and  $c$  is the heat capacity  $\partial E/\partial T$  in the vicinity of the transition. The latent heat  $q$  is equal to the horizontal part of the caloric curve, as indicated in the middle column of Fig. 4.

In order to simulate the photofragment spectra, the distributions for different numbers of absorbed photons are added and then smoothed to account for the broadening due to the fragmentation process. This gives the fragmentation pattern (grey curve) shown in the second line. The third line of Fig. 4 shows the corresponding calculated temperature dependence.

If now the photon energy nearly equals  $\Gamma$ , the fragment mass spectrum becomes structureless near  $T_m$  if the caloric curve is steplike. For any kind of smoothed out step in the caloric curve (left column in Fig. 4) the energy distributions are sharper and stay just separable even at  $T_m$ . In the case of a backbending caloric curve the energy distribution becomes bimodal and thus broader than in the case of the steplike curve. The calculated temperature dependence of the fragment mass spectra (third row of Fig. 4) show qualitatively different patterns for the cases of smoothed out or backbending caloric curves; i.e., the line joining the fragment group maxima shows a bend either to the right or to the left. This difference is influenced neither by the

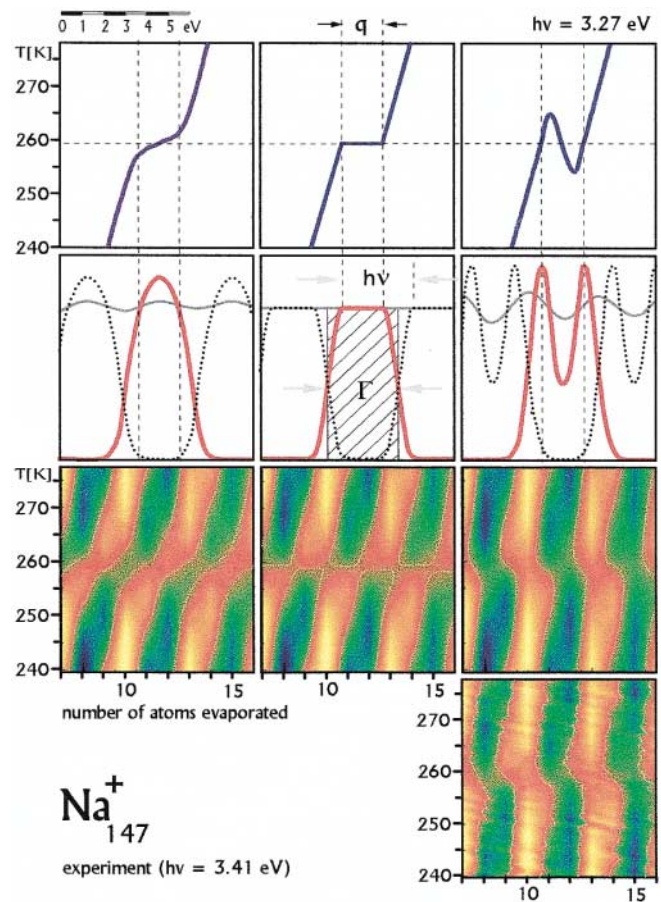


FIG. 4 (color). For a certain photon energy the bimodal envelopes of the photofragment groups can be made visible even in mass spectra strongly smoothed by the photofragmentation process, as is demonstrated here. The three caloric curves in the upper line agree in their latent heat  $q$ , melting temperature  $T_m$ , as well as the heat capacity in the vicinity of the transition, but they show a different behavior near  $T_m$ . The corresponding energy distributions are shown in red (and dotted black) in the second line, and the calculated fragmentation patterns in the third line. If the photon energy  $h\nu$  is now chosen to be nearly equal to the width  $\Gamma$  of the energy distribution of the steplike caloric curve, all structure in the fragment spectrum vanishes near  $T_m$  (middle column). In contrast, any backbending caloric curve leads to the characteristic pattern shown in the right column which is clearly different from the pattern of a smoothed out curve (left column). The lower figure shows the experimental data at the decisive photon energy of 3.41 eV. Only the pattern of a backbending caloric curve is reconcilable with the experiment.

experimental broadening nor by the specific shape of the backbending or smoothed caloric curves.

In order to do this special measurement one has to know  $\Gamma$ . We thus first measure data fields similar to those of Fig. 2 for different photon energies, and extract from them the melting temperature  $T_m$ , heat capacity  $c$ , and latent heat  $q$ . For  $\text{Na}_{147}^+$  this gives  $\Gamma = 3.27 \pm 0.14$  eV from Eq. (3). Then choosing a photon energy slightly higher than  $\Gamma$ , we remeasure the data set around  $T_m$ . If now the maxima in the data set bend to the left—like in the right column of Fig. 4—the energy distributions must be bimodal. This can indeed be seen in the experimental

data for  $h\nu = 3.41$  eV, shown in the lowest row of Fig. 4. Thus  $\text{Na}_{147}^+$  has an entropy with an inverted curvature and consequently a negative heat capacity in the energy range of the phase transition. A quantitative estimate for this heat capacity can be obtained from a least squares fit [19] to the data: at the melting temperature an increase of the internal energy of  $\text{Na}_{147}^+$  by 1 eV leads to a concomitant decrease in temperature by about 10 K.

How can this negative heat capacity be interpreted? Upon melting, a large system converts added energy completely into potential energy, reducing continuously the fraction of its solid phase. The kinetic energy and thus the temperature remain constant. A small system, on the other hand, tries to avoid partly molten states and prefers to convert some of its kinetic energy into potential energy instead. Therefore the cluster can become colder, while its total energy increases.

Negative heat capacities have now been found for melting clusters, fragmenting nuclei, and astronomical objects. What do these widely different systems have in common? The answer is that in these systems energy is not an extensive quantity; i.e., if such a system is divided into arbitrary subsystems the total energy is not simply the sum over the subsystems. The interaction between the subsystems has to be taken into account [2,14,15]. For example, in stars it is impossible to neglect the gravity between parts of the system [1,2]. Similarly in clusters and nuclei the interaction between subsystems is not negligible due to their small size.

The work was supported by the Deutsche Forschungsgemeinschaft through SFB 276.

---

[1] W. Thirring, *Z. Phys.* **235**, 339 (1970).

- [2] D. Lynden-Bell, *Physica* (Amsterdam) **263A**, 293 (1999).  
 [3] M. Bixon and J. Jortner, *J. Chem. Phys.* **91**, 1631 (1989).  
 [4] P. Labastie and R.L. Whetten, *Phys. Rev. Lett.* **65**, 1567 (1990).  
 [5] D. H. E. Gross, *Rep. Prog. Phys.* **53**, 605 (1990).  
 [6] M. D'Agostino *et al.*, *Phys. Lett. B* **473**, 219 (2000).  
 [7] M. Schmidt, R. Kusche, W. Kronmüller, B. v. Issendorff, and H. Haberland, *Phys. Rev. Lett.* **79**, 99 (1997).  
 [8] M. Schmidt, R. Kusche, B. v. Issendorff, and H. Haberland, *Nature* (London) **393**, 238 (1998).  
 [9] R. Kusche, Th. Hippler, M. Schmidt, B. v. Issendorff, and H. Haberland, *Eur. Phys. J. D* **9**, 1 (2000).  
 [10] G. Bertsch, *Science* **277**, 1619 (1997).  
 [11] R. S. Berry, *Nature* (London) **393**, 212 (1998).  
 [12] The melting temperatures given earlier [7–9] are 8 to 13 K too high, due to a malfunction of the temperature compensation of the electronic circuit reading the thermocouple for the thermalization cell. Corrected data are given in [13]. The melting temperature of  $\text{Na}_{147}^+$  deduced from Fig. 2 is  $259.1 \pm 1$  K.  
 [13] M. Schmidt *et al.*, in *Proceedings of the Nobel Symposium in Cluster Physics*, Visby (World Scientific, Singapore, to be published).  
 [14] L.D. Landau and E.M. Lifshitz, *Statistical Physics* (Pergamon Press, London, 1958).  
 [15] L. van Hove, *Physica* **15**, 951 (1949).  
 [16] C.L. Cleveland, U. Landman, T.G. Schaaf, M.N. Shafiqullin, P.W. Stephens, and R.L. Whetten, *Phys. Rev. Lett.* **79**, 1873 (1997).  
 [17] F. Calvo and F. Spiegelmann, *J. Chem. Phys.* **112**, 2888 (2000).  
 [18] A macroscopic system avoids the inverted curvature by phase separation, i.e., being partly liquid, partly solid, as described by the well known van Hove construction [1,2,5,15]. This is not advantageous for a small system, due to the large percentage of atoms at a liquid/solid interface.  
 [19] M. Schmidt *et al.* (unpublished).